

An experimental study of the spray from an air-assisted direct fuel injector

S H Jin^{1*}, M Brear¹, H Watson¹, and S Brewster²

¹Department of Mechanical Engineering, University of Melbourne, Parkville, Melbourne, Victoria, Australia

²Orbital Australia Pty Ltd, Balcatta, Western Australia, Australia

The manuscript was received on 6 September 2007 and was accepted after revision for publication on 12 June 2008.

DOI: 10.1243/09544070JAUTO710

Abstract: The transient behaviour of the fuel spray from an air-assisted direct-injection spark ignition (DISI) fuel injector has been investigated experimentally in a constant-volume chamber. As the chamber and injection pressures were varied, ensemble-averaged planar images of the laser-induced fluorescence (LIF) and Mie scattering from the spray were obtained to measure the Sauter mean diameter (SMD) using the laser sheet drop-sizing (LSD) technique. The root mean square (r.m.s.) SMD was also calculated by combination of the r.m.s. LIF and r.m.s. Mie scattering signals. The effect of the injection and chamber pressures and the ambient air density on the SMD, spray tip penetration, and dispersion of the air-assisted fuel injector are determined. In keeping with recent numerical studies by the group, vortex structures appear to be shed from the injector tip in back-illuminated images, indicating that the air and liquid motion are strongly coupled. These results also show that the spray penetration and SMD vary significantly with injection and chamber density, and scalings of the spray's overall SMD and penetration are proposed that achieve reasonable clustering in the experimental results.

Keywords: air-assisted direct fuel injector, direct-injection spark ignition, Sauter mean diameter, penetration, laser sheet drop sizing

1 INTRODUCTION

Substantial effort is currently being expended on improving the performance of gasoline-fuelled spark ignition (SI) engines, in order to meet ever-tightening emissions regulations while minimizing fuel consumption and carbon dioxide emissions. Such efforts include the manipulation of in-cylinder flow, optimization of the electronic control systems, and optimization of direct-injection spark ignition (DISI) fuel systems [1–4]. The improvements in fuel economy obtained by using DISI have prompted an increased adoption of this technology in passenger vehicles. Further study of fuel sprays in SI engines aims, in particular, to minimize the emissions of hydrocarbons (HCs), oxides of nitrogen (NO_x), and particulate matter (PM), and to improve efficiency through more complete combustion. Since the fuel

injection pressure of a DISI engine is typically lower than that of a diesel engine, larger fuel droplets can exist in the cylinder, and so slow evaporation may result. This is particularly the case during cold engine starting and warm-up, when the highest levels of HC emissions over the entire drive cycle occur. For these reasons, air-assisted direct fuel injectors with improved fuel atomization are currently under development.

Three main types of DISI design have been developed in recent years [5–7]. The 'wall-guided' injection system uses the piston crown to direct the fuel mixture towards the spark plug. This is the most common type of DISI engine today, and several manufacturers have this system in production. Recent work, however, has shown that the wall-guided injection can produce a relatively high amount of unburned HC and soot emissions, mainly owing to relatively poor mixture stratification at low loads and ineffective mixture homogenization at high loads [8]. The 'air-guided' injection system uses a well-defined gas motion, such as tumble,

*Corresponding author: Department of Mechanical Engineering, University of Melbourne, Parkville, Melbourne, Victoria, 3010, Australia. email: seongho@unimelb.edu.au

to transport the air–fuel mixture to the spark plug. The combustion is, however, often difficult to optimize for all loads and speeds [9]. A ‘spray-guided’ injection system does not require a surface or the in-cylinder air motion to control the stratification. The fuel spray is ignited at its periphery by a spark plug located close to the injector. Since the fuel concentration gradient along the periphery of the spray is relatively high, the spray shape has to be stable regardless of the in-cylinder processes. This injection system can therefore be quite sensitive to injector tolerances and the spray behaviour itself, e.g. the droplet diameter, spray penetration, and spray width.

The air-assisted direct-injection (DI) system studied in this paper is a form of spray-guided injection system. These systems have been previously reported to exhibit improvements in fuel consumption and HC emissions relative to multi-point port fuel injection in passenger vehicles [10]. The soot emissions were comparable with those of some wall-guided injection systems. A large reported advantage of a spray-guided injection system is that the stratified operating regime is considerably larger than for any other injection system. The air-assisted DI system also has several unique features compared with single-fluid injection systems. The most obvious of these is the addition of air, which is injected directly into the combustion chamber with the fuel. The pressure and quantity of the injected air influence the spray characteristics.

To date, however, there is relatively little published information on the performance of these air-assisted direct-injection systems. In particular, it is not at present clear what parametric effects air injection has on atomization and spray penetration. In some ways, air-assisted injection systems share similarities with so-called ‘effervescent atomizers’ designed for continuous injection in gas turbines and other devices [11, 12]. In both cases, the atomization process is more complex than for single-fluid injectors. However, the relative timing of the injected liquid and air phases in the air-assisted injector adds a further degree of freedom to its analysis.

In addition, the operation of an air-assisted DI system produces a dense spray and so also presents challenges in spray measurement. In almost all the studies discussed above, laser diffraction particle analysis (LDPA) and phase Doppler particle analysis (PDPA) were used to measure the droplet size, but there are disadvantages to both methods. LDPA is not suitable for dense spray measurement because of multiple-diffraction phenomena, and PDPA is used for point measurement; therefore, it needs substantial time and effort to obtain the droplet size

distribution across the whole spray. PDPA also suffers errors in measured mean drop size in dense sprays due to multiple occupancy of the measurement volume and to low signal-to-noise ratio due to multiple scattering. It is, therefore, worthwhile developing alternative methods, such as the planar imaging technique using a laser sheet in this paper, to study the transient spray characteristics [13–16].

This paper, therefore, presents an experimental study of an air-assisted direct fuel injector as a spray-guided injection system in a constant-volume chamber (CVC). Ensemble-averaged planar images of the laser-induced fluorescence (LIF) and Mie scattering from the spray are obtained to measure the Sauter mean diameter (SMD) while varying the injection and chamber pressure. The shot-to-shot variation in the spray structure is also obtained using a novel post-processing approach. Back-illuminated images are then obtained in the same conditions to observe the entire spray structure, and the penetration length and spray width are also determined from the laser images. Finally, scalings for the overall spray SMD and penetration are proposed that achieve reasonable clustering in the experimental results.

2 EXPERIMENTAL METHODS

The SMD can be determined for liquid droplets by combining the well-established techniques of Mie scattering and LIF. The intensity of the fluorescence signal measured by LIF is proportional to the concentration of the fluorescing molecules. As such, the observed fluorescence originates almost entirely from molecules in the liquid phase. The fluorescence intensity I_{LIF} per unit area of the emitted light is ideally proportional to the cube of the particle diameter, assuming negligible light absorption and negligible optical amplification [14], as given by

$$I_{\text{LIF}} = C_1 I_0 e^{-kx} \int_0^{\infty} D^3 \frac{dn}{dD} dD \quad (1)$$

where I_0 is the intensity of the incident laser beam, x is the distance travelled by the incident laser beam, k is an attenuation factor, D is the droplet diameter, dn is the droplet number density between D and $D+dD$, and C_1 is a constant that depends on the experimental configuration. In the case of significant absorption or optical amplification, I_{LIF} has been observed to vary with particle diameter to a power varying between 2.4 and 3.1 [14]. The exact relationship can only be established by examining a range of droplets of known diameter.

According to the Lorenz–Mie theory, the intensity of Mie scattering is a function of droplet diameter, the reflection rate of the droplet, polarization, and the wavelength of the incident beam. In the case of spherical droplets with a diameter larger than 1 μm and illuminated with a beam of wavelength 355 nm, the intensity is approximately proportional to the square of the droplet diameter [14] and can be expressed as

$$I_{\text{Mie}} = C_2 I_0 e^{-kx} Q_{\text{sca}} \int_0^\infty D^2 \frac{dn}{dD} dD \quad (2)$$

where C_2 is a coefficient determined by the characteristics of the detecting optical system and Q_{sca} is related to the angle between the incident laser beam and the detecting direction. Using equations (1) and (2), it is then found that the SMD is proportional to the ratio of the LIF intensity to the Mie intensity according to

$$\frac{I_{\text{LIF}}}{I_{\text{Mie}}} = \frac{C_1}{C_2 Q_{\text{sca}}} \frac{\int_0^\infty D^3 dn}{\int_0^\infty D^2 dn} = \frac{D_{32}}{C} \quad (3)$$

where $C = C_2 Q_{\text{sca}} / C_1$ has the units of length and can be determined with an appropriate calibration method, such as direction measurement, LDPA, or PDPA [16]. Importantly, the measurement of the LIF and Mie scattering signals using the same incident beam also yields a relative SMD of the spray that is not significantly related to the intensity profile of the incident laser sheet or its absorption because such effects should cancel for both measurements.

Because LIF and Mie scattering are captured sequentially, the instantaneous SMD could not be measured in the present set of experiments. Instead, both the LIF and the Mie images were ensemble averaged over 50 injection events, and larger number of ensembles did not yield significantly improved average images.

Ensemble averaging also allows some information on the shot-to-shot variation in the spray to be extracted from the images. Since the SMD is a function of two measured variables, the LIF and Mie scattered signals, its standard deviation can be determined from

$$\begin{aligned} \sigma_{\text{SMD}}^2 \approx & \sigma_{\text{LIF}}^2 \left(\frac{\partial \text{SMD}}{\partial I_{\text{LIF}}} \right)_{I_{\text{Mie}}}^2 + \sigma_{\text{Mie}}^2 \left(\frac{\partial \text{SMD}}{\partial I_{\text{Mie}}} \right)_{I_{\text{LIF}}}^2 \\ & + 2\sigma_{\text{LIF-Mie}}^2 \left(\frac{\partial \text{SMD}}{\partial I_{\text{LIF}}} \right)_{I_{\text{Mie}}} \left(\frac{\partial \text{SMD}}{\partial I_{\text{Mie}}} \right)_{I_{\text{LIF}}} \end{aligned} \quad (4)$$

Application of equations (1) to (3) then results in an

expression for the standard deviation of the SMD according to

$$\frac{\sigma_{\text{SMD}}^2}{\text{SMD}^2} = \frac{\sigma_{\text{LIF}}^2}{\text{LIF}^2} + \frac{\sigma_{\text{Mie}}^2}{\text{Mie}^2} - 2 \frac{\sigma_{\text{LIF-Mie}}^2}{\text{LIF} \times \text{Mie}} \quad (5)$$

with the non-dimensional root mean square (r.m.s.) of the SMD being the square root of equation (5). The third term on the right-hand side of equation (5) includes the cross-correlation of the LIF and Mie scattered signals. If the fluctuations measured in the LIF and Mie images are uncorrelated, this term vanishes [17]. This is the case in the present set of experiments, where the LIF and Mie images were taken separately and so cannot be correlated by definition.

Calculation of the SMD in this way avoids the requirement for simultaneous measurement of the LIF and Mie signals and is, therefore, desirable for reasons of both cost and complexity. However, care must be taken when considering the quantity σ_{SMD} ; the r.m.s. variation in a mean diameter appears to be a contradiction in terms. However, the laser sheet drop-sizing (LSD) technique, as summarized in equation (3) above, defines the SMD based on all droplets within each pixel. The SMD of a given pixel can vary at the same instant during different injection events. Thus, planar images showing the shot-to-shot variation in the SMD are meaningful over the entire injection cycle.

This extension of the laser sheet drop-sizing (LSD) technique to allow extraction of some information on the spray variation appears to be a novel aspect of the present experiments. In particular, if the histogram of droplet diameter D and number n of droplets at a given point in space and time are normal Gaussian, σ_{SMD} measured in this way is directly proportional to the r.m.s. of the droplet diameter D (σ_D) and the r.m.s. of the number of droplets (σ_n). Different relationships between σ_{SMD} , σ_D , and σ_n exist for other distributions, and the actual distributions cannot be determined using the present experimental approach.

Both ensemble-averaged LIF and ensemble-averaged Mie scattering images were not corrected for laser profile variation since the images and the profiles are divided to produce the relative SMD. The systematic laser profile features could therefore be cancelled across both the laser height and the thickness of the laser sheet. The SMD was calibrated by using PDPA at selected points throughout the spray in order to obtain the absolute SMD [18]. This calibration method, of course, has limitations be-

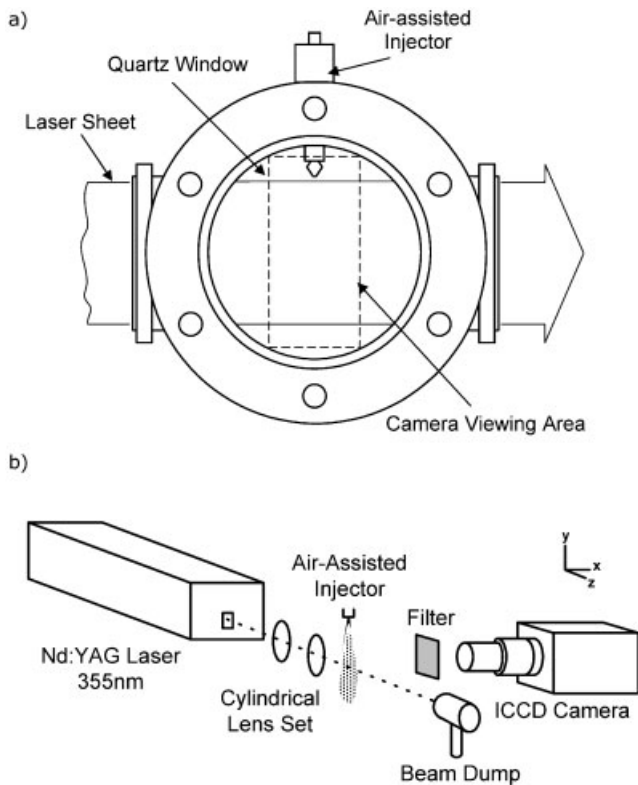


Fig. 1 (a) View of the CVC; (b) schematic diagram of the experimental set-up (Nd:YAG, neodymium-doped yttrium aluminium garnet; ICCD, intensified charge-coupled device)

cause the PDPA data themselves experience measurement error.

3 EXPERIMENTAL LAYOUT

A schematic diagram of the experimental set-up is shown in Fig. 1. The light source used was a neodymium-doped yttrium aluminium garnet (Nd:YAG) laser (Quantel, TwinsB). The laser pulse duration was 5 ns and the maximum energy was 120 mJ at a wavelength of 355 nm. A sheet beam was formed using a set of cylindrical lenses and the optical system was carefully aligned to minimize unwanted stray light, such as reflections from the chamber wall. The fluorescence and Mie scattered signals were imaged at a right angle to the laser beam using an intensified charge-coupled device (ICCD) camera (LaVision, FlowMaster3 with intensifier) with an ultraviolet Nikon lens ($f/\#$ 4.5) and a gate width of 100 ns. A GG-400 Schott glass filter was used for the fluorescence signal and a 355 nm band pass filter for Mie scattering. Then, 50 images of the LIF and Mie scattering at a given instant during subsequent injection events were ensemble averaged, with the back-

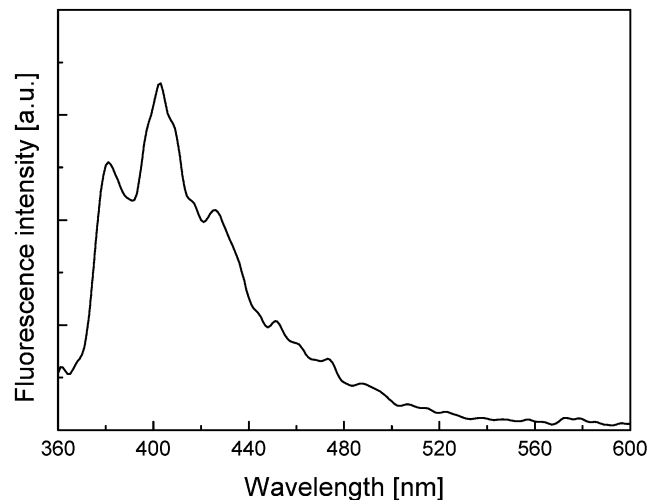


Fig. 2 LIF spectrum of the standard ULP used with excitation at 355 nm (a.u., arbitrary units)

ground subtracted and ratioed with the same alignment.

Standard unleaded petrol (ULP) with an octane number of 91 was used as the fuel during experiments. The LIF spectrum of this particular ULP blend when excited at 355 nm is broadband and ranges from 380 nm to 440 nm, with a peak at 405 nm (Fig. 2). The absorption coefficient of the ULP used in this experiment is approximately 30 mm^{-1} on excitation at a wavelength of 355 nm. Absorption and emission bands are spectrally well separated, ensuring the absence of fluorescence trapping and making possible the separation of the Mie scattered and the fluorescence signals. As reported previously, LIF has been applied to standard ULP sprays without seeding material, with the intensity proportional to the cube of droplet size, and the Mie scattering intensity proportional to the square of droplet size at an excitation wavelength of 355 nm [19].

The air-assisted direct-fuel-injection system consists of two main components: a fuel-metering injector, similar to a port fuel injector, and an air injector, which delivers a mixture of metered fuel and air into the CVC (Fig. 3). The fuel injector delivers fuel into a reservoir that is internal to the injector. The air injector then delivers this metered fuel into the chamber. The injector used has a projection as shown in Fig. 3(b). The maximum diameter of the projection is 6.43 mm, and fuel is injected around the projection at an angle of 60° . A unique feature of the system is the decoupling of the DI event with the fuel metering event, shown in Fig. 4. This allows the DI event to be tailored to the combustion requirements, rather than being limited by also needing to perform the fuel metering, as is

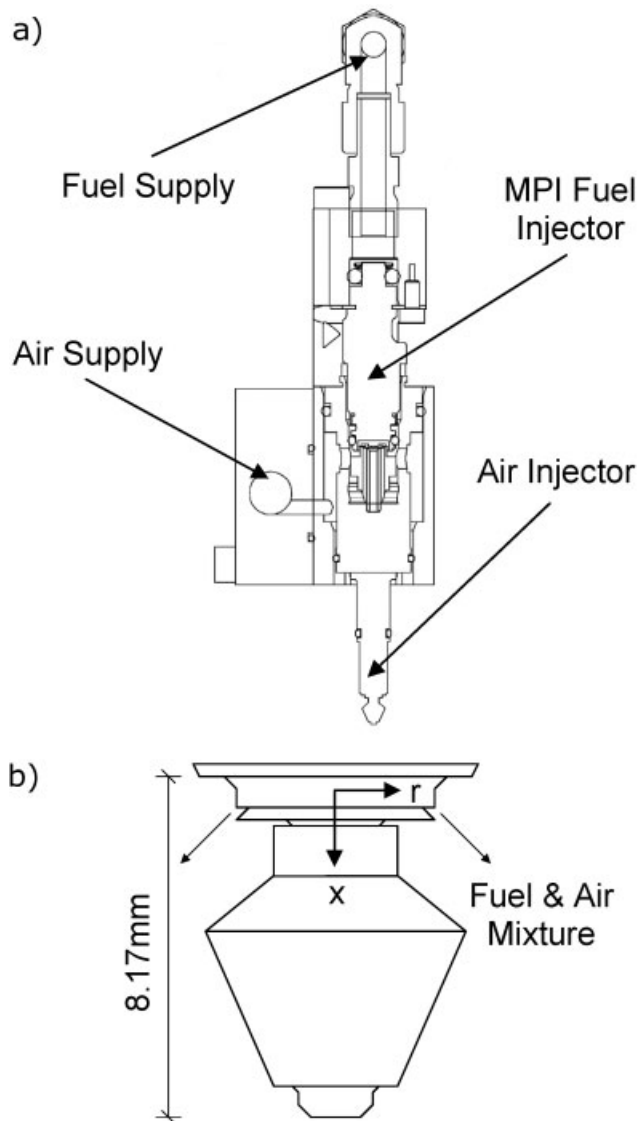


Fig. 3 Detailed diagrams of air-assisted, direct-fuel-injection system: (a) overall structure (MPI, multi-point injection); (b) details of the nozzle poppet

the case in high-pressure single-fluid-injection systems.

The chamber pressure, the air injection pressure, and the fuel injection pressure can all be varied independently in the present set of experiments (Table 1). Both fuel and air injection pressures were controlled by adjusting pressure regulators. The 3.78 l stainless steel cylinder was used as a fuel storage and pressure vessel for the injection. It holds more than 200 000 injection events as a batch without refilling of fuel, which was far more than was used in this study. The chamber pressure was also adjusted from atmospheric pressure up to 400 kPag. Pure nitrogen gas was used in order to

change the pressures of both the air injection and the chamber, and to minimize the fuel oxidation and quenching of the LIF signal. With a fuel injection duration of 3.085 ms at 800 kPag, approximately 10 mg of fuel was injected at a frequency of 0.5 Hz. Injection timing, laser triggering, and ICCD camera control were controlled by LabVIEW software. The times that are reported in this paper refer to the time after the trigger pulse was sent to the injector driver. This means that the first appearance of fuel is somewhat later owing to delays within the injector driver and the mechanical properties of the injector (Fig. 4). These unavoidable delays are typically a few hundred microseconds long and will be discussed later. The experiments were all performed at room temperature.

The CVC was formed by boring three perpendicular holes of 90 mm diameter into a single piece of mild steel slab. Each face of the chamber was then fitted with either quartz windows or blanking flanges. The air-assisted direct fuel injector is located in the top flange. Three quartz windows provide the optical access; two windows are for the laser sheet beam, and the other for the camera (Fig. 1(a)). The quartz windows permit full line-of-sight access to the chamber for optical diagnostics. The back flange has three ports: one for a pressure gauge to measure the chamber pressure, and two for intake and exhaust of ambient gas controlled by a solenoid valve. The time gap between injection events is 5 s. During that time gap, the residual gas and liquid fuel in the CVC are purged out via an automatically controlled solenoid valve. Sensitivity studies of the time gap showed that results did not change significantly when longer time gaps were used.

4 RESULTS AND DISCUSSION

4.1 Overall spray structure

Figure 5 shows the lift height of the nozzle tip against time after the start of air injection with different chamber pressures, ranging from atmospheric pressure to 600 kPag. These images were taken by focusing the ICCD camera on the injector seat. As mentioned earlier, there is a delay between the electrical triggering of the start and end of injection and the mechanical response of the injector (Fig. 4). The opening and closing delays for this injector were approximately 1.2 ms and 0.8 ms, respectively, at atmospheric pressure. Some nozzle tip bounce is also observed, although this is not expected to influence spray formation as only air

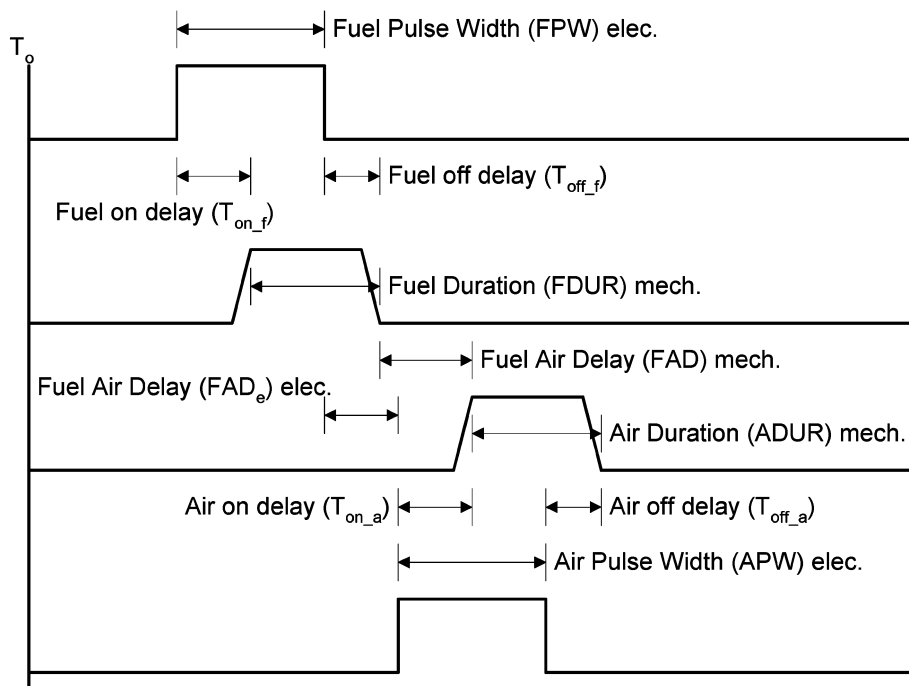


Fig. 4 Injection timing sequence

flows through the injector at this stage. Figure 5 also shows that, with increasing chamber pressure, the opening delay time increases and the closing delay time decreases for fixed electrical timing. This is because the net force acting on the injector acts in the direction of the chamber and decreases as the chamber pressure increases. These different lift histories should perhaps be taken into account when considering the transient spray development under various chamber pressures. Nonetheless, the maximum lift height is independent of chamber pressure, suggesting that such effects may be of secondary importance.

The SMD of the air-assisted direct fuel injector has been measured using planar laser-induced fluorescence (PLIF) and Mie scattering. Figure 6 shows single-shot and ensemble-averaged LIF, Mie scattering, and SMD images collected separately. These images were obtained 1.8 ms after the start of air injection for 800 kPag fuel injection pressure and 650 kPag air injection pressure (case 1 in Table 2).

Table 1 Data for the experimental conditions

Fuel injection pressure $P_{inj, fuel}$	800 kPag
Air injection pressure $P_{inj, air}$	650 kPag
Air pulse width	3.5 ms electrical
Air injection duration	3.0 ms mechanical
Fuel metering gain	10 mg/pulse
Fuel and air injection delay	1 ms mechanical
Chamber pressure P_{CVC}	0–400 kPag
Chamber temperature	Room temperature

The LIF image shows the liquid volume fraction, with most of the fuel mass in the centre of the spray. The Mie scattering image also has a strong signal in the centre of the spray but is narrower in width than the LIF image. Near the nozzle poppet, neither image is well defined because of surface scattering from the incident laser beam. The non-zero SMD above the injector tip in Fig. 6(b) is also mainly due to the surface scattering, and reflection of LIF and Mie scattering of the spray from the injector tip. This occurs even if spatial or bandpass filtering is used.

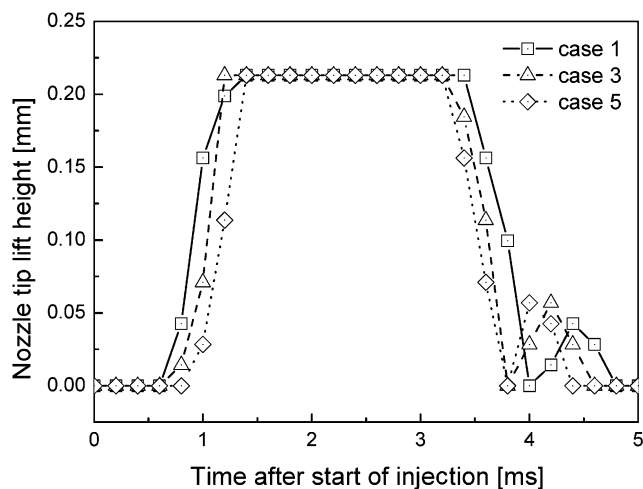


Fig. 5 Nozzle tip lift height with different CVC pressure versus time after the start of injection (electrical)

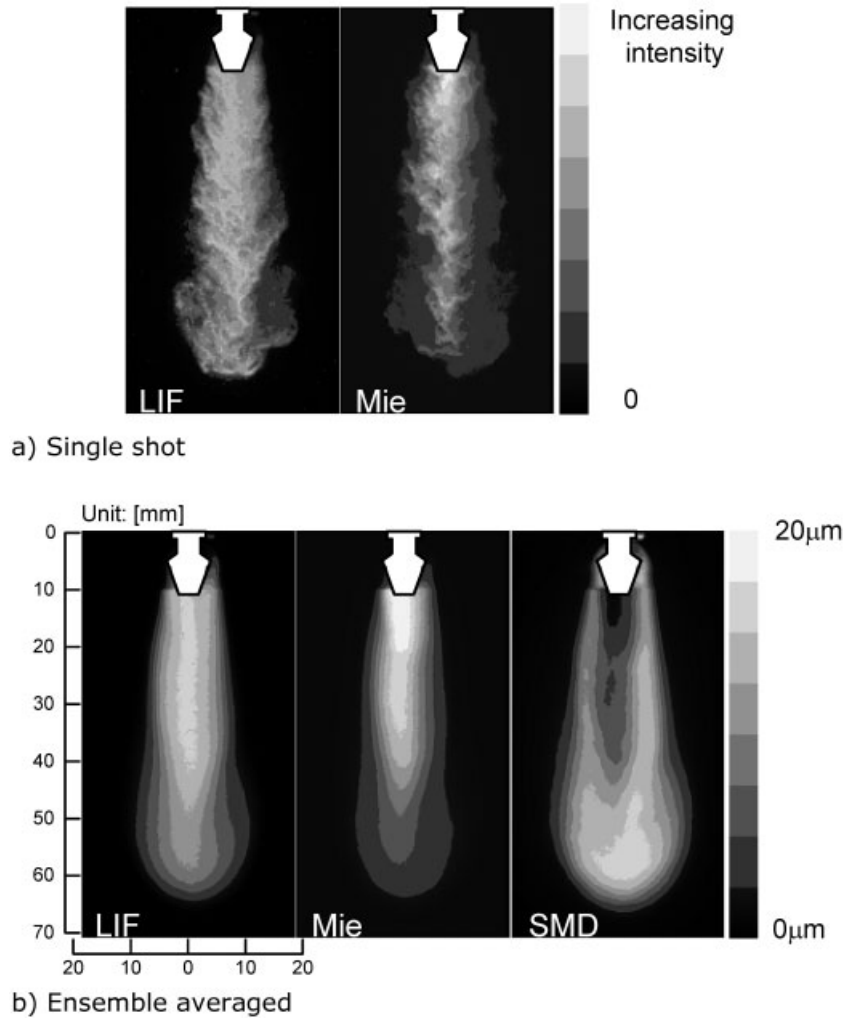


Fig. 6 (a) Single-shot and (b) ensemble-averaged images of LIF, Mie scattering, and SMD

As is shown in some detail in an associated paper [20], experiments and the numerical simulations feature local maxima in SMD either side of the injector centre-line. These regions can be seen to originate from the injector seat. This aspect of the numerical simulations was considered important because the experimental results for the SMD, such as in Fig. 6, are thought to be the first experimental results on this type of injector that shows this structure, and there was some initial concern that it was

an artefact of the LSD technique in this dense spray. This initial concern was based on the PLIF and Mie scattering images (e.g. Fig. 6(b)), from which the SMD is obtained, showing only a single peak along the injector centre-line. Thus, the agreement between the observed spray structures in the numerical simulations and experiments in this case supports the use of the LSD technique in this dense spray.

The SMD image possesses a degree of asymmetry about the injector centre-line, and such behaviour

Table 2 CVC, fuel, and air injection pressures for the cases studied

Case	Chamber pressure P_{CVC} (kPag)	Fuel injection pressure $P_{inj. fuel}$ (kPag)	Air injection pressure $P_{inj. air}$ (kPag)	$\Delta P_{air/CVC}$ $= P_{inj. air} - P_{CVC}$	Chamber density ρ_{CVC} (kg/m ³)
1	Atmospheric	800	650	650	1.2
2	100	800	650	550	2.4
3	200	800	650	450	3.6
4	300	800	650	350	4.8
5	400	800	650	250	6.0
6	150	950	800	650	3.0
7	300	1100	950	650	4.8

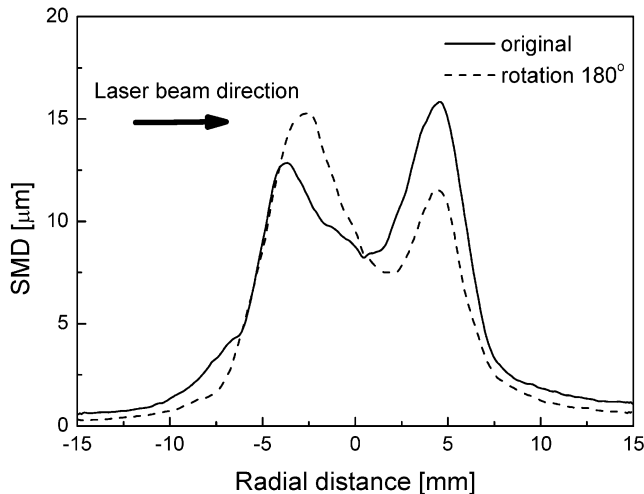


Fig. 7 SMD profiles at $x = 40$ mm with the injector in one orientation and then rotated by 180°

was seen throughout the present set of experiments. The results, presented in Fig. 7, show that similar asymmetric results were reflected when the injector was rotated 180° , thus demonstrating that this was due to non-axisymmetry in the experimental set-up, rather than in the measurement technique [20, 21].

A comparison between the SMD and r.m.s. SMD σ_{SMD} is shown in Fig. 8. Larger droplets are located in the periphery and front tip of the spray. A large value of the $\sigma_{\text{SMD}}/\text{SMD}$ is also observed in these regions. There are several effects that affect the calculation of the r.m.s. SMD, including the shot-to-shot variation in laser light intensity, number of droplets, and droplet size in the measuring volume on the r.m.s. SMD based on equations (1) and (2). The shot-to-shot variation in laser light intensity is about 2 per cent; the r.m.s. SMD is, therefore, mostly caused by the variation in the number of droplets and droplet size, especially in the spray tip and the edge of the spray in which the larger r.m.s. SMD was obtained.

That the r.m.s. variation in the SMD is a significant proportion of the local SMD is an important result in several respects. First, and most importantly, this shows that there is a degree of shot-to-shot variation in the spray, a feature which is expected to be common in other types of DISI systems as well. Further, this shot-to-shot variation has consequences for numerical modelling of the injection system. If quantities such as concentrations of soot, unburned HCs or NO_x are strongly and non-linearly dependent on the spray SMD, then modelling that assumes perfectly repeatable spray behaviour cannot be expected to give accurate absolute results.

Figure 9 shows the effect of chamber pressure on the ensemble-averaged SMD with various axial and

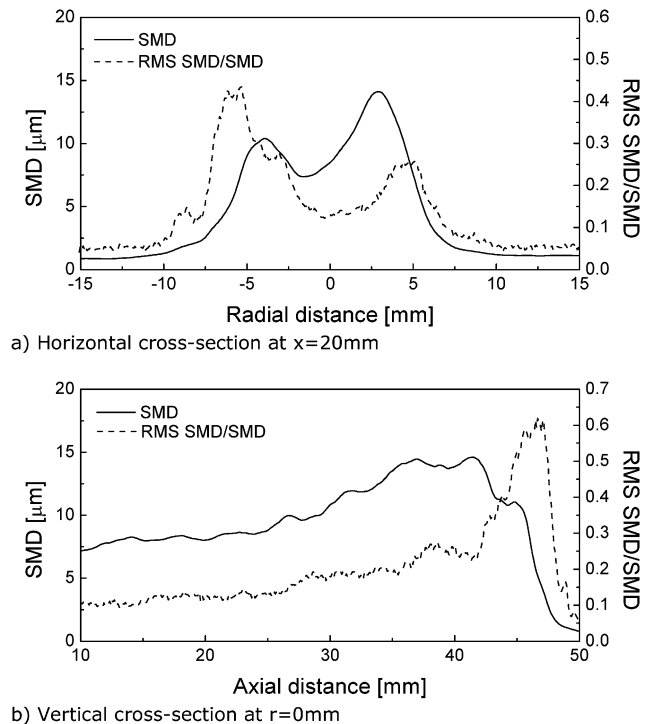


Fig. 8 Comparison of the SMD with the r.m.s. SMD, 1.5 ms after the start of injection (electrical)

radial distances. These images were measured 2.0 ms after the start of air injection with an 800 kPa fuel injection pressure and 650 kPa air injection pressure. As can be seen in this figure, there is a difference between the droplet sizes at locations such as the centre and periphery of the spray, and the droplet size is larger off the spray centre-line. This is thought to be because the larger droplets maintain their initial trajectory better because of their greater inertia, and is supported by numerical simulations in associated work by the group [20, 21]. The smaller droplets are deflected more by the air and so can migrate to the injector centre-line. The SMD also increases as the chamber pressure increases for constant fuel and air injection pressures.

4.2 Overall spray SMD

Since the SMD varies substantially over the entire spray, a measure of the overall SMD of the spray at a given instant can be obtained by area averaging according to

$$\text{Overall SMD} = \frac{1}{A} \int_A \text{SMD} \, dA \quad (6)$$

where A is defined as the area with non-zero SMD

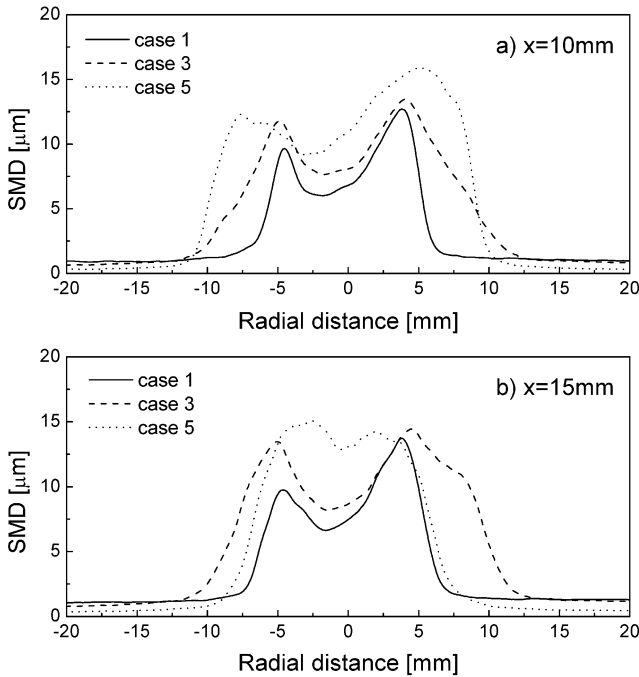


Fig. 9 SMD result with different CVC pressures, 2.0 ms after the start of injection (electrical)

and so increases with time after the start of injection. The overall SMD with various experimental conditions then is normalized on the basis of the overall SMD at the atmospheric pressure condition. The effect of the chamber pressure at different times after the start of injection on overall SMD is shown in Fig. 10. As is expected, the overall SMD increases to an extent with decreasing pressure difference between the injection and chamber pressures.

The overall SMD at a given instant is plotted versus the pressure ratio ($P_{CVC}/P_{inj, air}$) in Fig. 11, where results are normalized by the overall SMD at atmospheric chamber pressure. This figure should be interpreted keeping Fig. 10 in mind, which showed that the SMD did not vary a great deal over the injection period for a given test case. Figure 11 shows some clustering in the overall SMD data for the seven test cases, with cases 6 and 7 at substantially higher absolute injection pressures falling into the range of the other data. Several other non-dimensional parameters considered did not exhibit as much clustering. This suggests that it is the ratio of the injection pressure to the downstream pressure that is the main determinant of droplet diameter, which compares with the clear clustering in the spray penetration rate with a different non-dimensional parameter in the following section.

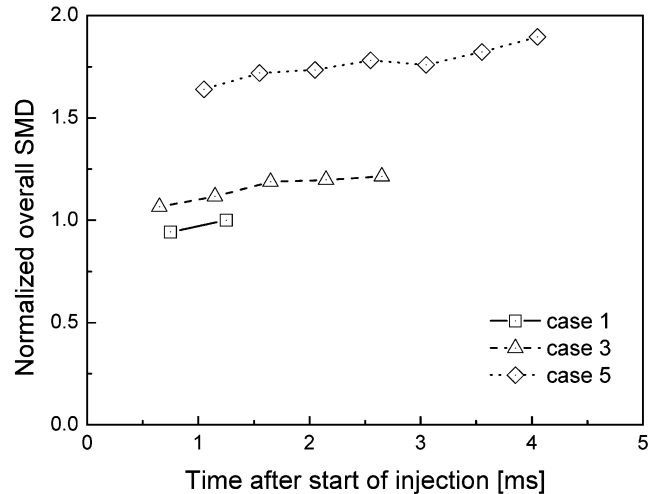


Fig. 10 Normalized overall relative SMD with different times after the start of injection (mechanical)

4.3 Spray penetration and width

Figure 12 shows back-illuminated images of the spray for different chamber pressures and electrical times after start of air injection. As discussed previously, because the delay between the electrical and mechanical opening times depended on the chamber pressure, the fuel discharge at the initial stage of injection (time after the start of injection, 1 ms) was slightly different. A strong coupling between the two injected phases and the chamber gas is implied in Fig. 12 by the appearance of an

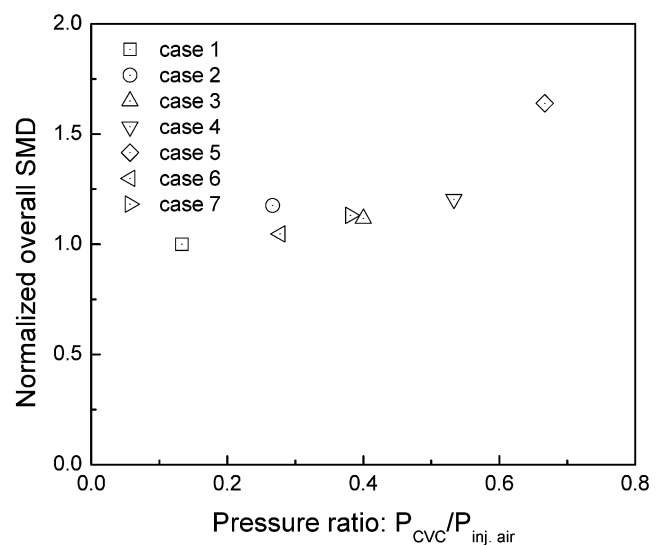


Fig. 11 Normalized overall SMD with different CVC and injection pressures at 2.0 ms after the start of injection (electrical)

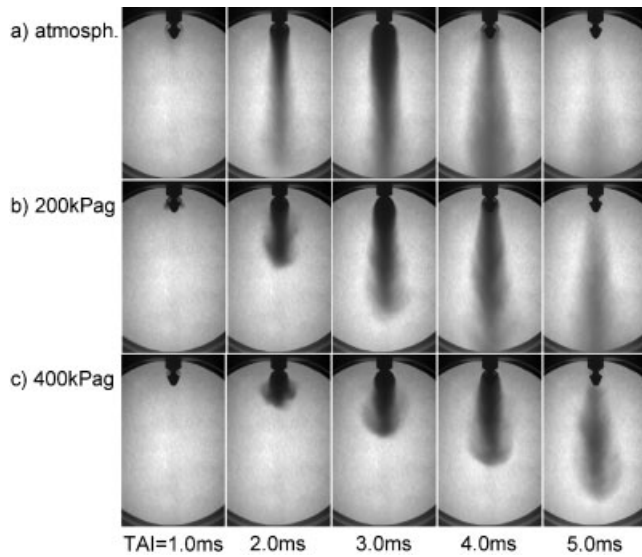


Fig. 12 Back-illuminated spray images with different CVC pressures at different times after the start of injection (TAIs)

‘arrowhead’ spray shape towards the end of injection, especially in the 400 kPag case. Numerical simulations on this injector performed by three of the present authors and co-workers in recent work [20–22] showed that this arrowhead shape arises from vortex rings that are shed from the injector at the start of injection, analogously to the shed vortex from a starting airfoil. This vortex ring translates away from the injector, carrying some liquid fuel around itself, which thereby generates the arrowhead shape.

The fuel spray penetration has an important influence on air utilization and fuel–air mixing rate in the combustion chamber, and Fig. 12 shows that it varies strongly over the test case studies. The spray tip penetration length was measured directly from the ensemble-averaged Mie scattering images, and was obtained by measuring the distance from the injector exit (Fig. 3(b)) to a certain range of the lower intensity Mie scattering contour in the axial direction (e.g. Fig. 6(b)). The maximum measured penetration was limited to 70 mm since the CVC had an internal diameter of 90 mm. Although not shown in this paper, a change in penetration rate occurred in all cases at about 80 mm, almost certainly owing to wall effects. The spray tip location might be also affected by the laser sheet profile in some degree.

Figure 13 shows the penetration length as a function of time for the different chamber pressures. The effect of varying the chamber pressure on the penetration is strong, but the rate of penetration is roughly constant over the entire injection event at a

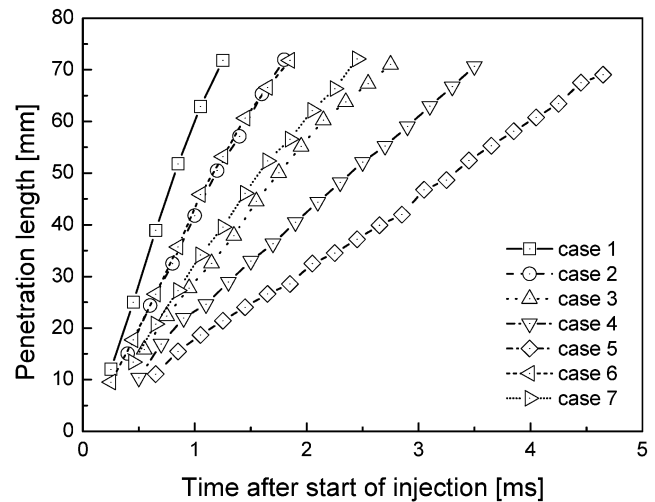


Fig. 13 Penetration length with different CVC and injection pressures as a function of time after the start of injection (mechanical)

given chamber pressure. It is noted, however, that varying the chamber pressure, while maintaining all other parameters, changes both the pressure difference between the injected fuel–air mixture and the chamber as well as the chamber density. Both of these were expected to be significant in determining penetration; therefore, Fig. 13 also shows two results, cases 6 and 7, in which the pressure difference between the fuel–air mixture and the chamber was maintained while the chamber pressure was increased from ambient. The penetration in both of these cases differs markedly from the matching case at ambient pressure.

A non-dimensional penetration rate can be formulated according to

$$\text{Non-dimensional penetration rate} = \frac{\text{penetration}}{\text{time}} \sqrt{\frac{\rho_a}{\Delta P}} \quad (7)$$

using the difference (ΔP) between the air injection and chamber pressures, the chamber density ρ_a , the measured spray penetration, and the mechanical time after the start of injection. This equation is similar to that used to investigate measurements of a diesel spray by Arai *et al.* [23]. Figure 14 shows this non-dimensional rate versus time after injection for all the results obtained, with clustering to within roughly 10 per cent of a mean value. Given the very large differences in the dimensional penetration with chamber pressure at any time after injection in Fig. 13, this clustering is significant. The clustering of test cases 6 and 7 with higher injection

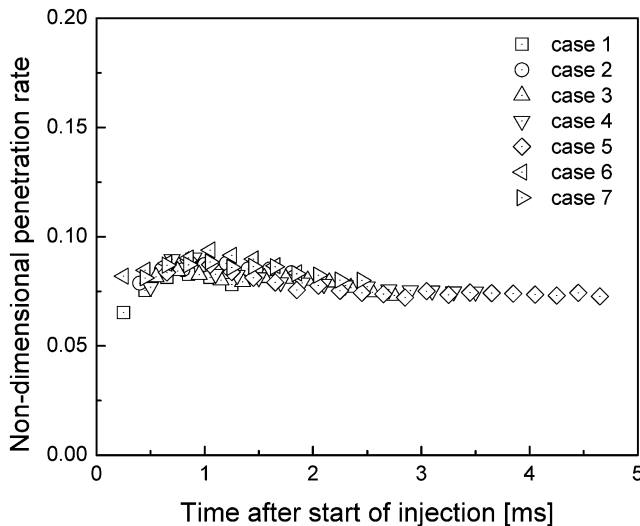


Fig. 14 Non-dimensional penetration rate versus time (mechanical)

pressures on to the data of other cases is of particular note.

Figure 15 shows the maximum spray width development as a function of the time after start of injection for different chamber and injection pressures. The clustering of this parameter over a broad range of operating conditions without any dimensional analysis was surprising to the present authors. It is nonetheless of practical significance, since it is desirable that these injectors can achieve a directed spray pattern over a broad range of operating conditions.

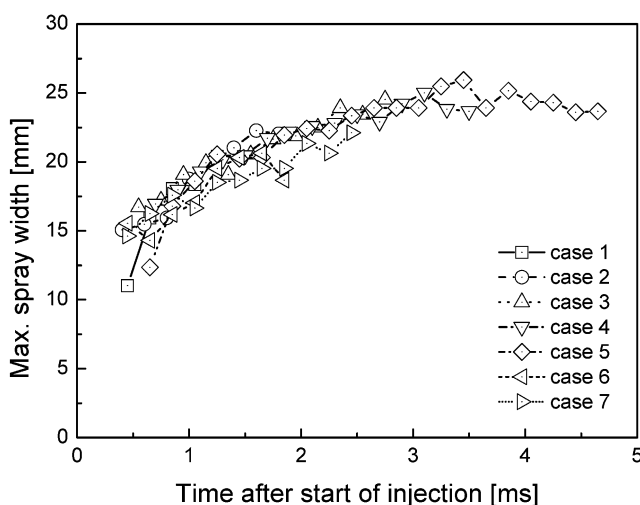


Fig. 15 Maximum spray width with different CVC and injection pressures as a function of time after the start of injection (mechanical)

5 CONCLUSIONS

The characteristics of the fuel spray from an air-assisted direct fuel injector have been obtained using optical techniques. The LSD technique, which required the combined use of Mie scattering and LIF, allowed determination of the SMD of the fuel spray. Both the Mie and the LIF images were ensemble averaged over separate injection events, thereby permitting study of the transient development of the ensemble averaged spray. The r.m.s. SMD, defined as the r.m.s. shot-to-shot variation in the SMD at a point in space, was determined by using the r.m.s. LIF and r.m.s. Mie scattering signals and found to be a significant fraction of the local SMD in some cases.

Several interesting aspects of the transient spray behaviour were noted. Spray containment enabled by the air assist was observed, with the spray maintaining a relatively narrow width that was insensitive to chamber pressure as it penetrated into the chamber. The largest droplets were also observed to lie off the spray centre-line, which was in agreement with recent numerical simulations performed by the group. This latter result was argued to support the utility of the planar LSD technique in this dense spray over some other spray diagnostic techniques. Back-illuminated images showed evidence of vortex rings shed from the injector, which appeared to become more apparent as the chamber pressure increased. This was also in agreement with recent numerical simulations performed by the group, and suggests that the air and liquid motion are strongly coupled.

Two non-dimensional parameters that described the overall spray development were proposed. The first was the ratio of the air injection pressure to the chamber pressure, which was found to be the main parameter controlling the SMD of the spray. The second used the difference between the air injection and chamber pressures, as well as the chamber density, to non-dimensionalize the spray penetration rate. Clustering with this second parameter was particularly good. The spray width was found to be insensitive to the chamber or injection pressures.

ACKNOWLEDGEMENTS

This work was supported financially by Orbital Australia Pty Ltd, Holden Limited, the Australian Research Council, and the Advanced Centre for Automotive Research and Testing. The authors are particularly grateful for the strong co-operation of

their industrial partners, as well as the technical support from Mr D. Halpin and Mr T. Grange.

REFERENCES

- 1 **Zhao, F. Q., Lai, M. C., and Harrington, D. L.** The spray characteristics of automotive port fuel injection – a critical review. SAE paper 950506, 1995.
- 2 **Sampson, M. J. and Heywood, J. B.** Analysis of fuel behaviour in the spark-ignition engine start-up process. SAE Paper 950678, 1995.
- 3 **Drake, M. C. and Haworth, D. C.** Advanced gasoline engine development using optical diagnostics and numerical modeling. *Proc. Combust. Inst.*, 2007, **31**, 99–124.
- 4 **Landenfeld, T., Kufferath, A., and Gerhardt, J.** Gasoline direct injection – SULEV emission concept. In *Direct injection SI engine technology 2004*, Special Publication SP-1832, 2004, SAE paper 2004-01-0041 (SAE International, Philadelphia, Pennsylvania).
- 5 **Iwamoto, Y., Noma, K., Nakayama, O., Yamauchi, T., and Ando, H.** Development of gasoline direct injection engine. SAE paper 970541, 1997.
- 6 **Kano, M., Saito, K., Basaki, M., Matsushita, S., and Gohno, T.** Analysis of mixture formation of direct injection gasoline engine. SAE paper 980157, 1998.
- 7 **Fry, M., King, J., and White, C.** A comparison of gasoline direct injection systems and discussion of development techniques. In *Direct injection SI engine technology 1999*, Special Publication SP-1416, 1999, SAE paper 1999-01-0171 (SAE International, Philadelphia, Pennsylvania).
- 8 **Drake, M. C., Fansler, T. D., and Lippert, A. M.** Stratified-charge combustion: modeling and imaging of a spray-guided direct-injection spark-ignition engine. *Proc. Combust. Inst.*, 2005, **30**, 2683–2691.
- 9 **Watson, H. C.** Professional development short course: road transport engine emission. Course Notes, SAE, Australia, Melbourne, 2005.
- 10 **Cathcart, G. and Zavier, C.** Fundamental characteristics of an air-assisted direct injection combustion system as applied to 4-stroke automotive gasoline engines. In *Direct injection SI engine technology 2000*, Special Publication SP-1499, 2000, SAE paper 2000-01-0256 (SAE International, Philadelphia, Pennsylvania).
- 11 **Sovani, S. D., Sojka, P. E., and Lefebvre, A. H.** Effervescent atomization. *Prog. Energy Combust. Sci.*, 2001, **27**, 483–521.
- 12 **Lefebvre, A. H.** Energy considerations in twin-fluid atomization. *ASME Trans., J. Engng Gas Turbine Power*, 1992, **114**, 89–96.
- 13 **Yeh, C., Kosaka, H., and Kaminoto, T.** Fluorescence/scattering image technique for particle sizing in unsteady diesel spray. *JSME Trans. B*, 1993, **59**, 308–313.
- 14 **LeGal, P., Farrugia, N., and Greenhalgh, D. A.** Laser sheet dropsizing of dense sprays. *Optics Laser Technol.*, 1999, **31**, 75–83.
- 15 **Stojkovic, B. C. and Sick, V.** Evolution and impingement of an automotive fuel spray investigated with simultaneous Mie/LIF techniques. *Appl. Phys. B*, 2001, **73**, 75–83.
- 16 **Jermey, M. C. and Greenhalgh, D. A.** Planar dropsizing by elastic and fluorescence scattering in sprays too dense for phase Doppler measurement. *Appl. Phys. B*, 2000, **71**, 703–710.
- 17 **Taylor, J. R.** *An introduction to error analysis*, 1997 (University Science Books, Sausalito, California).
- 18 **Cathcart, G., Houston, R., and Ahern, S.** The potential of gasoline direct injection for small displacement 4-stroke motorcycle applications. SAE paper 2004-32-0098, 2004.
- 19 **Park, S., Cho, H., Yoon, I., and Min, K.** Measurement of droplet size distribution of gasoline direct injection spray by droplet generator and planar image technology. *Measmt Sci. Technol.*, 2002, **13**, 859–864.
- 20 **Boretti, A. A., Jin, S. H., Zakis, G., Brear, M. J., Attard, W., Watson, H. C., Carlisle, H., and Bryce, W.** Experimental and numerical study of an air assisted fuel injector for a D.I.S.I. engine. In *Direct injection SI engine technology, 2007*, Special Publication SP-2084, 2007, SAE paper 2007-01-1415 (SAE International, Philadelphia, Pennsylvania).
- 21 **Boretti, A. A., Jin, S. H., Zakis, G., Brear, M. J., Attard, W., Watson, H. C., Carlisle, H., and Bryce, W.** Experimental and numerical study of a spark ignition engine with air assisted, direct injection. *Proc. IMechE, Part D: J. Automobile Engineering*, 2008, **222**(6), 1103–1119.
- 22 **Murdoch, P., Wigley, G., Heath, J., and Pitcher, G.** A combined CFD and experimental analysis of the spray produced by an air-assisted GDI injector. In *Proceedings of the 16th Annual Conference on Liquid atomization and spray systems (ILASS Europe 2000)*, Darmstadt, Germany, September 2000 (ILASS-Europe ONLVS, Naples).
- 23 **Arai, M., Tabata, M., Hiroyasu, H., and Shimizu, M.** Disintegrating process and spray characterization of fuel jet injected by a diesel nozzle. SAE paper 840275, 1984.